J. Fluid Mech. (2016), *vol.* 786, *pp.* 294–308.
doi:10.1017/jfm.2015.673

Scale-to-scale energy and enstrophy transport in two-dimensional Rayleigh–Taylor turbulence

Quan Zhou[1,†], Yong-Xiang Huang[2], Zhi-Ming Lu[1], Yu-Lu Liu[1] and Rui Ni[3]

[1]Shanghai Institute of Applied Mathematics and Mechanics, and Shanghai Key Laboratory of Mechanics in Energy Engineering, Shanghai University, Shanghai 200072, China

[2]State Key Laboratory of Marine Environmental Science, Xiamen University, Xiamen 361102, China

[3]Department of Mechanical and Nuclear Engineering, The Pennsylvania State University, University Park, PA 16802-1412, USA

(Received 16 May 2015; revised 25 October 2015; accepted 9 November 2015; first published online 2 December 2015)

We apply a recently developed filtering approach, i.e. filter-space technique (FST), to study the scale-to-scale transport of kinetic energy, thermal energy, and enstrophy in two-dimensional (2D) Rayleigh–Taylor (RT) turbulence. Although the scaling laws of the energy cascades in 2D RT systems follow the Bolgiano–Obukhov (BO59) scenario due to buoyancy forces, the kinetic energy is still found to be, on average, dynamically transferred to large scales by an inverse cascade, while both the mean thermal energy and the mean enstrophy move towards small scales by forward cascades. In particular, there is a reasonably extended range over which the transfer rate of thermal energy is scale-independent and equals the corresponding thermal dissipation rate at different times. This range functions similarly to the inertial range for the kinetic energy in the homogeneous and isotropic turbulence. Our results further show that at small scales the fluctuations of the three instantaneous local fluxes are highly asymmetrically distributed and there is a strong correlation between any two fluxes. These small-scale features are signatures of the mixing and dissipation of fluids with steep temperature gradients at the fluid interfaces.

Key words: buoyancy-driven instability, turbulent convection, turbulent mixing

1. Introduction

Rayleigh–Taylor (RT) instability can occur when a layer of heavier fluid is placed on top of a layer of lighter fluid in a gravitational field. The evolution of RT instability would result in the so-called RT turbulence, in which the kinetic energy of the mixed fluid layer increases at the expense of the potential energy and the spectra of velocity fluctuations cover a broad range of scales. The process is relevant in a wide variety of fields in nature and engineering, such as filamentary structures in the heating of the solar corona (Isobe *et al.* 2005), buoyancy-driven mixing in the atmosphere and oceans and in cloud formation, thermonuclear flames in type Ia supernovae (Zingale *et al.* 2005; Cabot & Cook 2006), and fuel–pusher mixing in inertial confinement

† Email address for correspondence: qzhou@shu.edu.cn

fusion (Taleyarkhan *et al.* 2002). In addition, this system provides a fascinating fluid-mechanical framework for the study of non-stationary turbulent flows.

Despite the great importance and the long history of RT turbulence, there are still some open issues (Dimonte *et al.* 2004; Abarzhi 2010*b*). One important issue in the field is to determine the dynamics that drive the cascades of turbulent fluctuations at small scales inside the mixing layer. This has been extensively studied in the past in both two-dimensional (2D) and three-dimensional (3D) RT systems (Dalziel, Linden & Youngs 1999; Zhou 2001; Wilson & Andrews 2002; Chertkov 2003; Celani, Mazzino & Vozella 2006; Matsumoto 2009; Boffetta *et al.* 2009, 2010, 2012; Vladimirova & Chertkov 2009; Abarzhi 2010*a*; Biferale *et al.* 2010; Chung & Pullin 2010; Soulard 2012; Soulard & Griffond 2012; Zhou 2013; Qiu, Liu & Zhou 2014).

Specifically, in two dimensions, Chertkov (2003) argued that the traditional inverse kinetic energy and direct enstrophy cascades, long proposed for 2D Navier–Stokes turbulence (Clercx & van Heijst 2009; Boffetta & Ecke 2012), are both not realizable in 2D RT turbulence. Instead, Chertkov (2003) adopted the Bolgiano–Obukhov (BO59) scenario to resolve the small-scale spatial temporal correlations of the velocity and temperature fields. In the BO59 scenario, the buoyancy force is assumed to balance the inertial force at all scales smaller than the energy-containing scale. Taking this together with the thermal balance between the thermal transfer and dissipation rates, one obtains the BO59 scaling, i.e.

$$S_p(r,t) \equiv \langle u_r(t)^p \rangle \sim r^{3p/5} t^{-p/5} \quad \text{and} \quad R_p(r,t) \equiv \langle \theta_r(t)^p \rangle \sim r^{p/5} t^{-2p/5}, \tag{1.1a,b}$$

for pth-order velocity and temperature structure functions, $S_p(r,t)$ and $R_p(r,t)$. Here, u_r and θ_r are, respectively, the velocity and temperature increments over a separation r and $\langle\cdot\rangle$ indicates a volume average inside the mixing layer. This spatiotemporal scaling (1.1) was numerically verified first by Celani *et al.* (2006) and then by a scale-by-scale study of Biferale *et al.* (2010). Later, Zhou (2013) tested quantitatively the force balance relation and revealed that the buoyancy force balances the inertial force at all scales below the integral length scale. The numerical work of Zhou (2013) thus validates the basic force balance assumption of the BO59 scenario in 2D RT turbulence.

Besides the scaling behaviour (1.1), the scale-to-scale transport is of fundamental importance in turbulence phenomenology, especially for 2D turbulence (Boffetta & Ecke 2012). Celani *et al.* (2006) first pointed out that within the so-called inertial range of 2D RT turbulence, the kinetic energy is driven by a backward transfer due to buoyancy forces while the temperature variance obeys a classical forward cascade. This was later retrieved from the Monin–Yaglom relation by the theoretical work of Soulard (2012). The direction of the kinetic energy cascade was numerically investigated by Boffetta *et al.* (2012). In a 3D RT system of high aspect ratio, in which one transverse side is much smaller than the others, Boffetta *et al.* (2012) observed a transition from 3D to 2D turbulent behaviour with the increasing scale, when the height of the mixing layer becomes larger than the scale of confinement. In particular, they revealed that for scales sufficiently large the third-order velocity structure function becomes positive, signalling an upscale kinetic energy transfer at these scales.

In this paper, we want to deepen the previous understanding by focusing on the scale-to-scale energy and enstrophy transport in 2D RT turbulence. As stated above, temperature becomes a fully active scalar in 2D RT turbulence, leading to the

emergence of a BO59 scaling. This is dramatically different from the 3D situation, where temperature behaves as a passive scalar and hence the Kolmogorov-like (K41) phenomenology was predicted (Chertkov 2003; Soulard 2012) and observed (Matsumoto 2009; Boffetta *et al.* 2010; Boffetta & Musacchio 2010). It is thus of great interest to investigate the spectral transfer process in such a non-K41 system, and this is why we focus on the 2D geometry in the present work.

Three considerations prompted us to perform the present investigation. First, although the direct cascade of temperature variance is theoretically expected for incompressible velocities, independently of the active/passive character of the temperature field, it has not been examined in 2D RT turbulence, to the best of our knowledge. In addition, the thermal balance plays an important role in BO59 phenomenology (Chertkov 2003) and thus needs to be directly validated. Second, the enstrophy cascade has not been studied in the framework of RT turbulence, and clarifying its direction is of fundamental interest and importance. Finally, how to connect the spatiotemporal details of the spectral transfer process with coherent structures is an important yet unknown question, which cannot be approached using the traditional structure function method, as they are spatially averaged quantities.

Here, we apply the filter-space technique (FST) (Germano 1992; Liu, Meneveau & Katz 1994; Eyink 1995; Borue & Orszag 1998; Rivera *et al.* 2003) to our numerical data set of 2D RT turbulence. Recently, FST has received much attention in revealing the spectral transfer properties of the double cascade in 2D turbulence (Rivera *et al.* 2003; Chen *et al.* 2003, 2006; Boffetta 2007; Xiao *et al.* 2009; Boffetta & Musacchio 2010; Wan *et al.* 2010; Kelley & Ouellette 2011; Liao & Ouellette 2013, 2014) and it has been further proved to be a very efficient technique even for the poorly resolved velocity field (Ni, Voth & Ouellette 2014). The basic idea of FST is not difficult to understand: when small-scale components are removed from nonlinear equations by a low-pass spatial filter, some new terms arise to describe the coupling and interaction between the filtered small scales and the retained large scales. Therefore, these new terms can be used to characterize the transfer of a given quantity between scales in turbulence.

Using FST, we will show that even though a new type of phenomenology, i.e. the BO59 scenario, was theoretically predicted and indeed numerically confirmed in 2D RT turbulence, the kinetic energy is still transferred to large scales by an inverse cascade, as already reported by Boffetta *et al.* (2012), while both the thermal energy and enstrophy are driven by forward cascades. Moreover, we will reveal the local features of the three instantaneous fluxes, including their asymmetrical distributions and strong correlations at small scales. These local small-scale features correspond to the mixing and dissipation near the interfaces between hot and cold plumes.

The remainder of this paper is organized as follows. In § 2, we give a brief description of our numerical methods and filtering techniques. The results are presented and analysed in § 3, and we summarize our findings and conclude in § 4.

2. Methods

2.1. *Governing equations and numerical model*

We consider the spatial temporal evolution of a single component fluid in two dimensions. At the beginning ($t = 0$), the colder uniform fluid is placed above the hotter uniform fluid with an initial temperature jump Θ_0, and the velocity is zero

everywhere. The system is then governed by the Oberbeck–Boussinesq equations

$$\frac{\partial u_j}{\partial t} + u_i \frac{\partial u_j}{\partial x_i} = -\frac{\partial p}{\partial x_j} + \nu \frac{\partial^2 u_j}{\partial x_i^2} + \beta g \delta_{j2} \theta, \tag{2.1}$$

$$\frac{\partial \theta}{\partial t} + u_i \frac{\partial \theta}{\partial x_i} = \kappa \frac{\partial^2 \theta}{\partial x_i^2}, \tag{2.2}$$

$$\frac{\partial u_i}{\partial x_i} = 0, \tag{2.3}$$

for the velocity field $\boldsymbol{u}(\boldsymbol{x}, t)$, the kinematic pressure field $p(\boldsymbol{x}, t)$, and the temperature field $\theta(\boldsymbol{x}, t)$. Here, summation is implied over double indices, δ_{ij} is the Kronecker symbol, g is the acceleration of gravity, and β, ν and κ are, respectively, the thermal expansion coefficient, kinematic viscosity and thermal diffusivity of the working fluid. In the horizontal direction, periodic boundary conditions are used for both the velocity and temperature fields. No-slip velocity and no-flux temperature boundary conditions are adopted for the top and bottom walls.

To reveal the properties of scale-to-scale energy and enstrophy transport, the time evolution of the velocity $\boldsymbol{u}$, temperature θ, and vorticity ω $(= \boldsymbol{\nabla} \times \boldsymbol{u})$ fields is investigated by means of direct numerical simulations. The numerical method has been described in detail in Zhou (2013) and Huang & Zhou (2013), hence we give only its main features here. The Oberbeck–Boussinesq equations (2.1)–(2.3) are solved in their vorticity–stream function formulation on a 2D domain of height L_z with uniform grid spacing using a finite-difference scheme (Liu, Wang & Johnston 2003). An essentially compact fourth-order scheme (Weinan & Liu 1996) is employed to discretize the momentum equation, with the gravity term treated explicitly. The temperature transport equation (2.2) is solved using fourth-order long-stencil difference operators. The classical third-order Runge–Kutta method is applied to integrate both the momentum and temperature equations in time, and the time step is chosen to fulfil the Courant–Friedrichs–Lewy conditions.

In the present study, a spatial resolution of 4096×8193 grid points is used to adequately resolve the small-scale properties. To assess the repeatability of the statistical quantities, a total of 32 independent realizations have been produced by adding different perturbations to the initial temperature interface. All statistical quantities studied in this paper are thus obtained by first calculating for each individual realization and then averaging over all these simulations. In all the runs, $Ag = 0.25$, $L_z = 1$, $\Theta_0 = 1$, $\nu = \kappa = 2.89 \times 10^{-6}$ and $Pr = 1$, where $A = (\beta\Theta_0)/2$ is the Atwood number and $Pr = \nu/\kappa$ is the Prandtl number.

During the RT evolution, a layer of mixed fluid develops and grows in time. Figure 1(*a*) depicts a typical snapshot of the instantaneous temperature field in a 4096^2 subregion inside the mixing layer obtained in a late stage of RT evolution (at $t/\tau = 4$, where $\tau = \sqrt{L_z/Ag}$ is the characteristic time of the system). The corresponding velocity and vorticity fields are shown in figure 1(*b*). The growth of the mixing layer can be characterized by its height, $h(t)$, defined as a vertical layer where $-0.4\Theta_0 \leqslant \langle\theta(\boldsymbol{x}, t)\rangle_x \leqslant 0.4\Theta_0$, with $\langle\theta(\boldsymbol{x}, t)\rangle_x$ being the horizontally averaged temperature profiles. The temporal evolution of $h(t)$ has been studied in our previous work (see figure 1 of Qiu *et al.* 2014). It is found that there is a self-similarity turbulent range $1.6 \lesssim t/\tau \lesssim 4$ within which $h(t)$ follows the accelerated law $h(t) \sim t^2$ and the spectra of both velocity and temperature fluctuations cover a broad range of scales. Various time-averaged global quantities and small-scale statistical properties

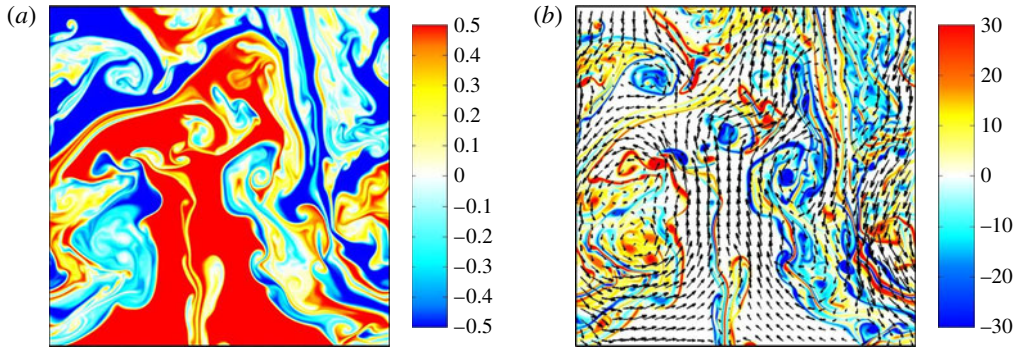

FIGURE 1. (*a*) Snapshot of the instantaneous temperature field in a 4096^2 subregion at $t/\tau = 4$. Blue regions indicate the cold fluid, while red regions correspond to the hot fluid. (*b*) The corresponding velocity (arrows) and vorticity (colour) fields. Blue colours identify the negative values, while red colours mark the positive values.

within this self-similarity range have been reported previously (Zhou 2013; Qiu *et al.* 2014). Here, we apply a new analysis to the data and study the scale-to-scale energy and enstrophy transport using FST.

2.2. *Filter-space techniques*

For 2D RT turbulence, we consider the convolution,

$$f^{(r)}(\boldsymbol{x}) = \int G^{(r)}(\boldsymbol{x} - \boldsymbol{x}') f(\boldsymbol{x}')\, \mathrm{d}\boldsymbol{x}', \tag{2.4}$$

as a low-pass filtered field, where $f = u_i$, θ and ω for velocity, temperature and vorticity, respectively, $G^{(r)}$ is chosen to be a round Gaussian filter, and the superscript (r) indicates a quantity containing the information from contributions only at length scales larger than r. With these filtered quantities, one can define the filtered kinetic energy to be $E^{(r)} = (u_i^{(r)} u_i^{(r)})/2$, the thermal energy to be $\Theta^{(r)} = (\theta^{(r)}\theta^{(r)})/2$, and the enstrophy to be $\Omega^{(r)} = (\omega^{(r)}\omega^{(r)})/2$, and the evolution equations for $E^{(r)}$, $\Theta^{(r)}$ and $\Omega^{(r)}$ are, respectively, given by

$$\frac{\partial E^{(r)}}{\partial t} = -\frac{\partial J_i^{(r)}}{\partial x_i} - \nu \frac{\partial u_i^{(r)}}{\partial x_i}\frac{\partial u_i^{(r)}}{\partial x_i} + \beta g \delta_{i2} u_i^{(r)} \theta^{(r)} - \Pi^{(r)}, \tag{2.5}$$

$$\frac{\partial \Theta^{(r)}}{\partial t} = -\frac{\partial K_i^{(r)}}{\partial x_i} - \kappa \frac{\partial \theta^{(r)}}{\partial x_i}\frac{\partial \theta^{(r)}}{\partial x_i} - N^{(r)} \tag{2.6}$$

and

$$\frac{\partial \Omega^{(r)}}{\partial t} = -\frac{\partial L_i^{(r)}}{\partial x_i} - \nu \frac{\partial \omega^{(r)}}{\partial x_i}\frac{\partial \omega^{(r)}}{\partial x_i} + \beta g \delta_{i1} \omega^{(r)} \frac{\partial \theta^{(r)}}{\partial x_i} - Z^{(r)}. \tag{2.7}$$

Here, $J_i^{(r)}$, $K_i^{(r)}$ and $L_i^{(r)}$ are spatial currents of $E^{(r)}$, $\Theta^{(r)}$ and $\Omega^{(r)}$, respectively, and the terms containing $J_i^{(r)}$, $K_i^{(r)}$ and $L_i^{(r)}$ do not change the net budget, but spatially redistribute energy and enstrophy in the resolved scales, i.e the scales larger than r. The terms proportional to ν and κ are sink terms that denote direct dissipation of

filtered energy and enstrophy due to the effects of viscosity and thermal diffusivity. The terms proportional to βg are source terms that represent the kinetic energy and enstrophy injections due to the buoyancy effects. The final terms on the right-hand sides, given by

$$\Pi^{(r)} = -[(u_i u_j)^{(r)} - u_i^{(r)} u_j^{(r)}] \frac{\partial u_i^{(r)}}{\partial x_j}, \tag{2.8}$$

$$N^{(r)} = -[(u_i \theta)^{(r)} - u_i^{(r)} \theta^{(r)}] \frac{\partial \theta^{(r)}}{\partial x_i} \tag{2.9}$$

and

$$Z^{(r)} = -[(u_i \omega)^{(r)} - u_i^{(r)} \omega^{(r)}] \frac{\partial \omega^{(r)}}{\partial x_i}, \tag{2.10}$$

are the scale-to-scale fluxes, respectively, of $E^{(r)}$, $\Theta^{(r)}$ and $\Omega^{(r)}$ across the filter scale r. These terms originate from the filtering of the nonlinear terms in the equations and express the coupling and interaction between the removed scales and the retained scales. With the above definitions, negative values for $\Pi^{(r)}$, $N^{(r)}$ and $Z^{(r)}$ denote the transfer of energy and enstrophy from scales $<r$ to scales $>r$, while positive values imply the opposite transfer process.

3. Results and discussion

Figure 2(*a–f*) shows examples of instantaneous scale-to-scale flux fields of $\Pi^{(r)}$, $N^{(r)}$ and $Z^{(r)}$ across two different filter scales, i.e. $r = 1.9\eta$ around the viscous scale η and $r = 60.5\eta$ within the inertial range. These fields are computed using the filtering procedure as described in § 2.2 from the same velocity, temperature and vorticity fields as in figure 1, and normalized by their respective standard deviations $\Pi_{sd}^{(r)}$, $N_{sd}^{(r)}$ and $Z_{sd}^{(r)}$. In the figures, red regions represent positive flux, while blue regions mark negative flux. One sees that the spatial distributions of these instantaneous fluxes are strongly inhomogeneous. When a relatively small filter scale r is chosen, as shown in figure 2(*a–c*), linelike regions of intense (positive or negative) flux appear. These linelike structures seem to originate from the interfaces between hot and cold fluids, and we will return to this issue at the end of this section. The intense-flux regions become larger and smoother with increasing r (see, e.g. figure 2*d–f*), as more of the small-scale components are removed for a larger filter scale. In addition, regions of both inverse and forward cascades are observed for $\Pi^{(r)}$, $N^{(r)}$ and $Z^{(r)}$, i.e. locally all these quantities can be transferred either to smaller scales or to larger scales.

To quantify the details of local fluxes, the probability density functions (PDFs) of kinetic energy $\Pi^{(r)}$, thermal energy $N^{(r)}$ and enstrophy $Z^{(r)}$ fluxes, for three different filter scales $r = 1.9\eta$, 14.2η and 60.5η, are calculated and plotted in figure 2(*g–i*). It is seen that fluctuations of the kinetic energy flux $\Pi^{(r)}$ are asymmetric, with the negative fluctuations being larger than the positive ones, and the level of this asymmetry becomes higher for smaller scales. The net gain of the negative fluctuations thus implies a mean inverse cascade of kinetic energy from small to large scales. The similar features can be revealed for the PDFs of $N^{(r)}$ and $Z^{(r)}$, except that the positive fluctuations of the two fluxes are both larger than their negative counterparts, suggesting a mean direct cascade of both thermal energy and enstrophy from large to small scales.

The asymmetry of the local fluxes distribution can be quantitatively measured by their skewness. Figure 3(*a–c*) plots the flux skewness $\Pi_{skewness}^{(r)}$, $N_{skewness}^{(r)}$ and $Z_{skewness}^{(r)}$ as

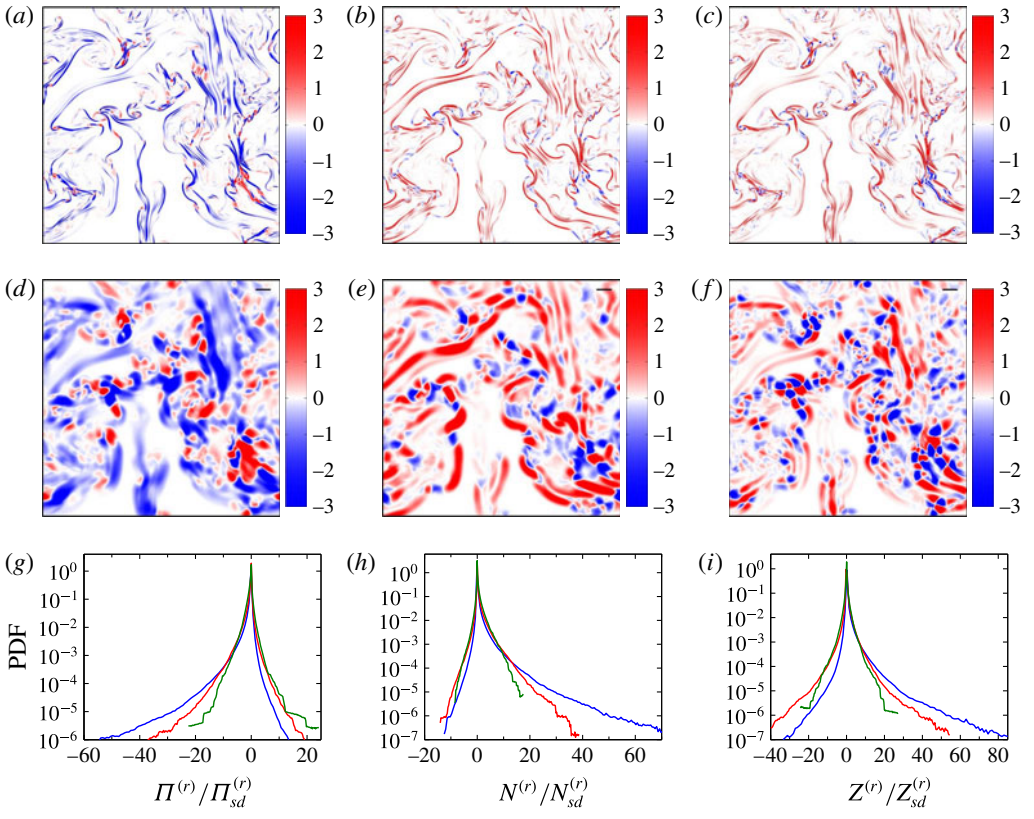

FIGURE 2. (*a–f*) Instantaneous spatial distributions of scale-to-scale (*a*,*d*) kinetic energy flux $\Pi^{(r)}$, (*b*,*e*) thermal energy flux $N^{(r)}$ and (*c*,*f*) enstrophy flux $Z^{(r)}$ across the scales (*a–c*) $r = 1.9\eta$ and (*d–f*) $r = 60.5\eta$ obtained from the same velocity, temperature and vorticity fields as in figure 1, with each normalized by its standard deviation. Red colours mean the transfer of energy and enstrophy to smaller length scales, while blue colours denote the transfer to larger scales. (*g–i*) PDFs of (*g*) kinetic energy $\Pi^{(r)}$, (*h*) thermal energy $N^{(f)}$ and (*i*) enstrophy $Z^{(r)}$ fluxes, normalized respectively by their standard deviations $\Pi^{(r)}_{sd}$, $N^{(r)}_{sd}$ and $Z^{(r)}_{sd}$, through different filter scales r.

a function of the filter scale at three different evolution times $t/\tau = 2$, 3 and 4. Three features are worthy of note: (i) all skewness of $\Pi^{(r)}$ are negative, while $N^{(r)}_{skewness}$ and $Z^{(r)}_{skewness}$ are positive for most of scales; (ii) their magnitudes decrease continuously to zero with increasing filter scale r, suggesting symmetric fluctuations of these fluxes at large scales; (iii) the maximum skewness magnitude occurs at small scales and this maximum increases with increasing evolution time t. Note that the present observed PDFs, especially for small scales, seem to be more asymmetric than those measured in other 2D turbulence systems (Rivera *et al.* 2003; Chen *et al.* 2006; Boffetta 2007). This may be attributed to the buoyancy effects in 2D RT turbulence. For example, from flow visualizations (Qiu *et al.* 2014) we found that small thermal structures are more likely to merge and group together to form large-scale structures, and during this process the kinetic energy, supplied by buoyancy forces at small scales, goes primarily to large scales.

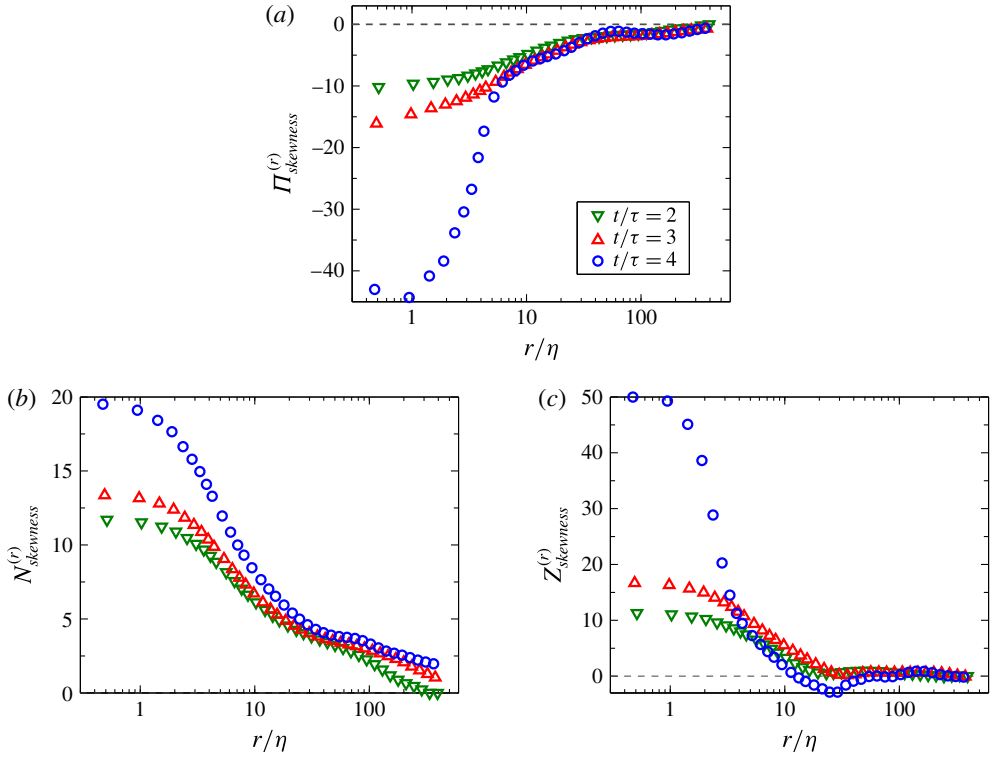

FIGURE 3. (Colour online) Skewness of (*a*) kinetic energy flux $\Pi^{(r)}$, (*b*) thermal energy flux $N^{(r)}$ and (*c*) enstrophy flux $Z^{(r)}$ as a function of the normalized filter scale r/η at times $t/\tau = 2$, 3 and 4.

We now turn to the mean energy and enstrophy transport. Figure 4(*a*) shows in a log–log plot the negative value of the spatially averaged kinetic energy flux, $-\langle\Pi^{(r)}\rangle$, as a function of the filter scale at times $t/\tau = 2$, 3 and 4. A negative flux of kinetic energy is observed for all times and over all scales studied, indicating that the kinetic energy is transferred, on average, to large scales, as first pointed out by Celani *et al.* (2006) and theoretically expected by Soulard (2012). This result agrees well with the conclusion of an upscale kinetic energy transfer, for scales sufficiently large in a quasi-2D RT system, revealed from the third-order velocity structure function by Boffetta *et al.* (2012). Taking this result together with those obtained in previous works (Celani *et al.* 2006; Biferale *et al.* 2010; Boffetta *et al.* 2012; Zhou 2013), we can now try to sketch the cascade picture of kinetic energy in 2D RT turbulence. As shown in figure 4(*b*), the kinetic energy, injected by buoyancy term $\beta g\theta_r u_r$ on scale r, cascades upwards to larger scales. The BO59 scenario would require the balance $\beta g\theta_r u_r \sim \Pi^{(r)} \sim u_r^3/r$, which has been verified to be valid for all scales below the integral length scale (Zhou 2013). As indicated by Lohse & Xia (2010) in their review paper, this balance implies that on scale r the kinetic energy obtained from smaller scales (such as from scale $r/2$) would be required to be negligible when compared with the energy transferred to larger scales (such as to scale $2r$), i.e. $|\langle\Pi^{(r)}\rangle| \gg |\langle\Pi^{(r/2)}\rangle|$. In the inset of figure 4, we plot the ratio between $|\langle\Pi^{(r)}\rangle|$ and $|\langle\Pi^{(r/2)}\rangle|$. It is seen

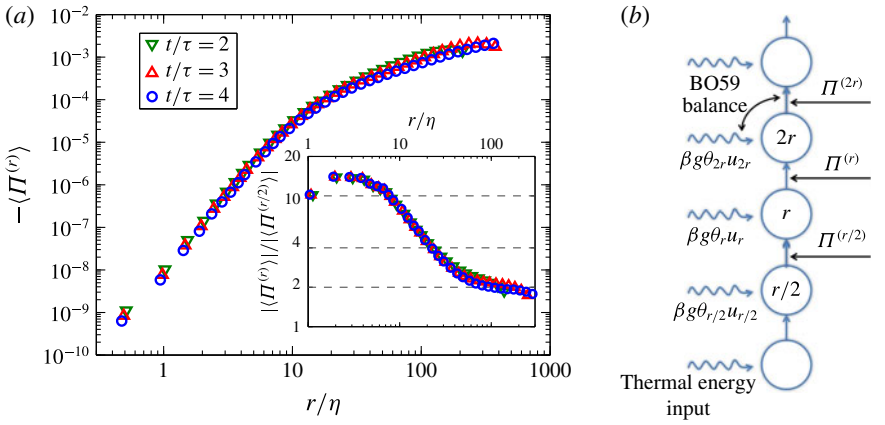

FIGURE 4. (Colour online) (*a*) The negative value of the mean kinetic energy flux, $-\langle \Pi^{(r)} \rangle$, as a function of the normalized filter scale r/η at times $t/\tau = 2$, 3 and 4. Inset: the ratio $|\langle \Pi^{(r)} \rangle|/|\langle \Pi^{(r/2)} \rangle|$. (*b*) Sketch of the BO59 cascade of kinetic energy in 2D RT turbulence. The sketch is adapted from figure 4(*b*) of Lohse & Xia (2010) for the three-dimensional Rayleigh–Bénard convection where the cascade is downscale. In the present case, kinetic energy, supplied by the buoyancy term $\beta g \theta_r u_r$ on scale r, is driven by a backward transfer.

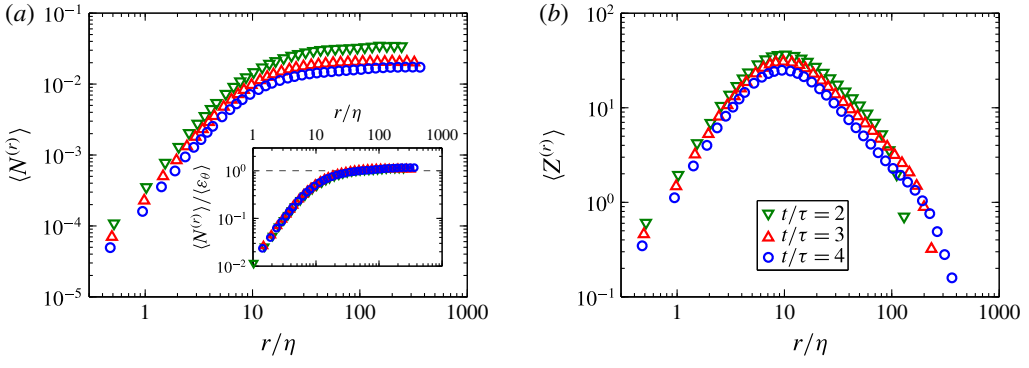

FIGURE 5. (Colour online) The mean (*a*) thermal energy $\langle N^{(r)} \rangle$ and (*b*) enstrophy $\langle Z^{(r)} \rangle$ fluxes as a function of the normalized filter scale r/η at times $t/\tau = 2$, 3 and 4. Inset of (*a*): $\langle N^{(r)} \rangle$ compensated by the spatially averaged thermal dissipation rate $\langle \varepsilon_\theta(t) \rangle$.

that $|\langle \Pi^{(r)} \rangle| > \langle \Pi^{(r/2)} \rangle|$ over all scales studied and $|\langle \Pi^{(r)} \rangle|$ is further larger than $4|\langle \Pi^{(r/2)} \rangle|$ for $r \lesssim 20\eta$.

Although the kinetic energy follows an inverse cascade due to the buoyancy effects, the temperature fluctuations, governed by the temperature advection equation (2.2), are expected to cascade continuously from large to small scales (Chertkov 2003; Lohse & Xia 2010; Soulard 2012). Figure 5(*a*) shows the spatially averaged thermal energy flux $\langle N^{(r)} \rangle$ as a function of filter scale at three evolution times. Positive values are definitely observed for $\langle N^{(r)} \rangle$ over all scales. Furthermore, the thermal energy flux seems to asymptote to a plateau value for scales $r \gtrsim 30\eta$, indicative of an inertial downscale transfer of thermal energy. Indeed, the thermal balance derived from (2.2)

requires that in the inertial range the thermal transfer rate is independent of the scale and is equal to the thermal dissipation rate, i.e.

$$\langle N^{(r)} \rangle \sim \langle \varepsilon_\theta \rangle, \tag{3.1}$$

where

$$\varepsilon_\theta(\boldsymbol{x}, t) \equiv \kappa [\partial \theta(\boldsymbol{x}, t)/\partial x_i]^2 \tag{3.2}$$

is the thermal dissipation rate. To test this balance, we plot in the inset of figure 5(*a*) the compensated thermal energy flux $\langle N^{(r)} \rangle / \langle \varepsilon_\theta \rangle$. After compensation, the three data sets gained at different times of RT evolution collapse almost perfectly on top of each other. And there is a reasonably extended range (over roughly one decade) through which the compensated thermal energy flux has an approximately constant value of unity. The presented results thus validate the thermal balance in 2D RT turbulence.

The spatial average of the enstrophy flux is plotted as a function of filter scale in figure 5(*b*). Again, positive values are seen for $\langle Z^{(r)} \rangle$ for all times and scales, indicating a direct cascade of enstrophy to small scales. This is qualitatively consistent with previous observations in other 2D flow systems (Rivera *et al.* 2003; Boffetta 2007; Liao & Ouellette 2014). Notice that the maximum of the enstrophy flux occurs at the scale $r \simeq 10\eta$, around which both the kinetic and thermal energy fluxes experience a transition, as shown in figures 4(*a*) and 5(*a*), respectively. The scale $r \simeq 10\eta$ is the approximate cross-scale between the inertial range and the viscous range (Zhou 2013). Therefore, the observed different behaviours of $\Pi^{(r)}$, $N^{(r)}$ and $Z^{(r)}$ above and below this scale are attributed to different statistical properties of these fluxes within different (i.e. inertial and viscous) ranges. Note also that, unlike other 2D turbulence systems, the energy and enstrophy cascades in 2D RT turbulence seem to operate in the same range of scales. This is because in 2D RT system the kinetic energy and enstrophy are simultaneously injected by buoyancy forces at all scales smaller than the energy-containing scale.

Next, we study the correlations among the three local fluxes. To explore this question, we calculated the cross-correlation coefficients $C_{\Pi N}(r)$ between $\Pi^{(r)}$ and $N^{(r)}$, $C_{\Pi Z}(r)$ between $\Pi^{(r)}$ and $Z^{(r)}$, and $C_{NZ}(r)$ between $N^{(r)}$ and $Z^{(r)}$, respectively, according to

$$C_{\Pi N}(r) = \frac{\langle (\Pi^{(r)} - \langle \Pi^{(r)} \rangle)(N^{(r)} - \langle N^{(r)} \rangle) \rangle}{\Pi_{sd}^{(r)} N_{sd}^{(r)}}, \tag{3.3}$$

$$C_{\Pi Z}(r) = \frac{\langle (\Pi^{(r)} - \langle \Pi^{(r)} \rangle)(Z^{(r)} - \langle Z^{(r)} \rangle) \rangle}{\Pi_{sd}^{(r)} Z_{sd}^{(r)}} \tag{3.4}$$

and

$$C_{NZ}(r) = \frac{\langle (N^{(r)} - \langle N^{(r)} \rangle)(Z^{(r)} - \langle Z^{(r)} \rangle) \rangle}{N_{sd}^{(r)} Z_{sd}^{(r)}}. \tag{3.5}$$

The dependence of the coefficients $C_{\Pi N}(r)$, $C_{\Pi Z}(r)$ and $C_{NZ}(r)$ on the filter scale at three evolution times is reported in figure 6(*a–c*). One sees that the coefficients are negative for $C_{\Pi N}(r)$ and $C_{\Pi Z}(r)$, but positive for $C_{NZ}(r)$. In general, the correlation is higher for smaller r than that for larger r. At small scales, the three fluxes are strongly correlated or anticorrelated. This can also be revealed by figure 2(*a–c*), from which it is easy to see that the scale-to-scale flux fields of $\Pi^{(r)}$, $N^{(r)}$ and $Z^{(r)}$ across the filter scale $r = 1.9\eta$ share similar linelike patterns, i.e. the intense energy and enstrophy fluxes appear nearly in the same physical regions. At large scales, however, the strength of the correlation becomes weaker.

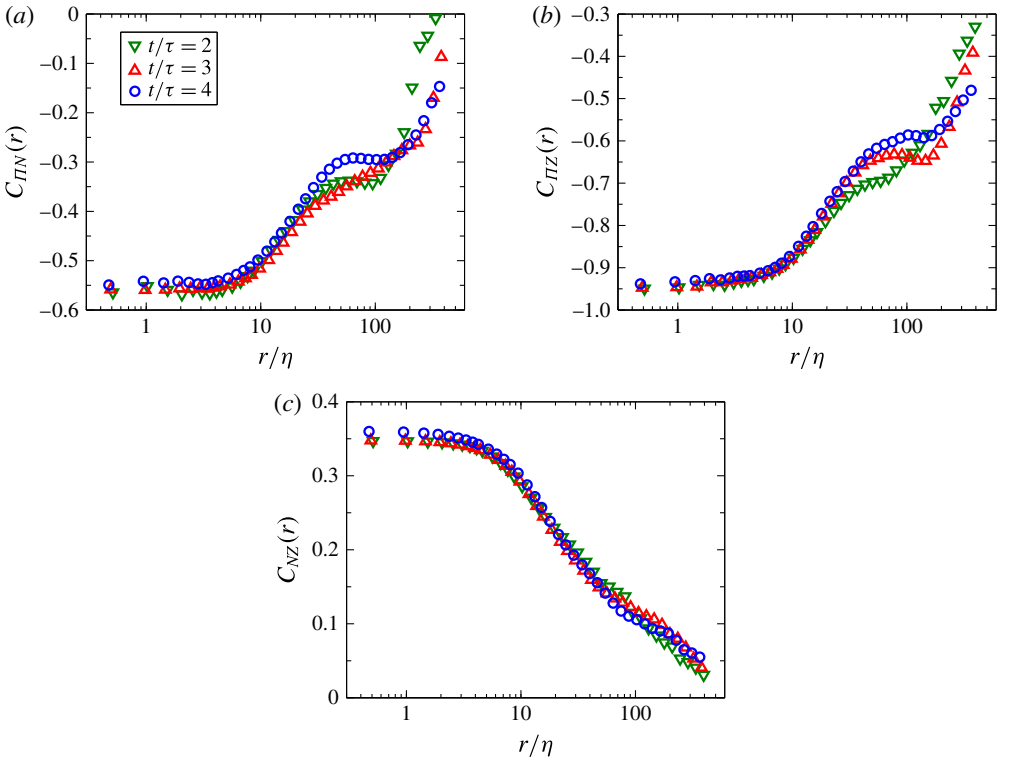

FIGURE 6. (Colour online) Cross-correlation coefficients (*a*) $C_{\Pi N}(r)$, (*b*) $C_{\Pi Z}(r)$ and (*c*) $C_{NZ}(r)$ as a function of the normalized filter scale r/η at times $t/\tau = 2$, 3 and 4.

The interpretation of the strong correlations among the three fluxes at small scales relies on the understanding of those linelike structures, as shown in figure 1(*a–c*). Unlike the spotty structures in other 2D turbulence systems, these structures are quite unique in 2D RT turbulence, suggesting that they may be related to some flow structures in our system. In two dimensions, a line can be used to separate an area into two distinct regions. In figure 1(*a*), the two regions can be physically interpreted as hot and cold plumes, and those lines seem to mark their interfaces. Figure 7(*a*) shows the instantaneous field of $\varepsilon_\theta(\boldsymbol{x}, t)$ calculated from the temperature field in figure 1(*a*). For comparison, we replot the figure 2(*b*) as figure 7(*b*). The red lines in figure 7(*a*) indicating large temperature gradients are very similar to those of the intense fluxes in figure 7(*b*). More quantitatively, the cross-correlation coefficient between the two reaches 0.8. This is a very large correlation considering that ε_θ is a positively defined quantity and the other one is not. Together with the large correlations among the three fluxes, it suggests that, at small scales, the intense fluxes are all located near the interfaces of cold and hot plumes.

In RT turbulence, the kinetic energy is siphoned from the potential energy by means of the invasion of cold and hot plumes into each other. The interface between the two will therefore evolve from a single horizontal straight line at the beginning to complex topological structures with large tortuosity. In the interfacial regions, the magnitudes of the various quantities, such as the temperature gradient as well as the shear between the two plumes moving in the opposite directions, should be large. Since it happens in a thin layer near the interface, these structures dominate the small-scale energy and

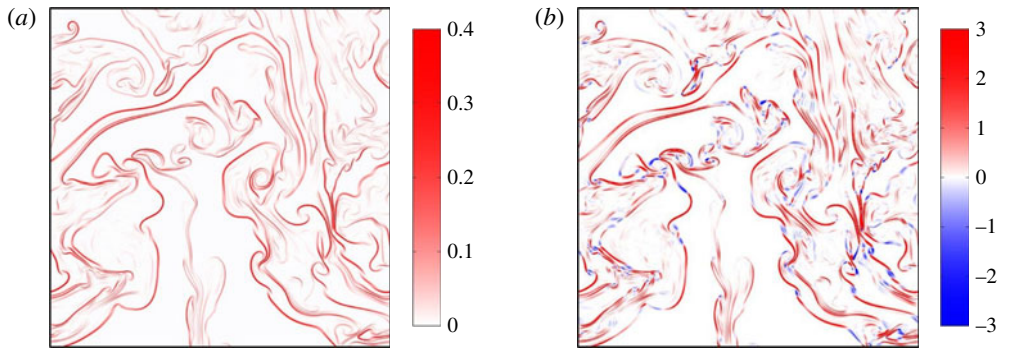

FIGURE 7. (*a*) Snapshot of the instantaneous field of thermal dissipation rate $\varepsilon_\theta(\boldsymbol{x}, t)$, corresponding to the temperature field in figure 1(*a*). Red colours indicate positions of large temperature gradients, and thus can be used to detect the interfaces between hot and cold fluids. (*b*) Replot of figure 2(*b*) for comparison.

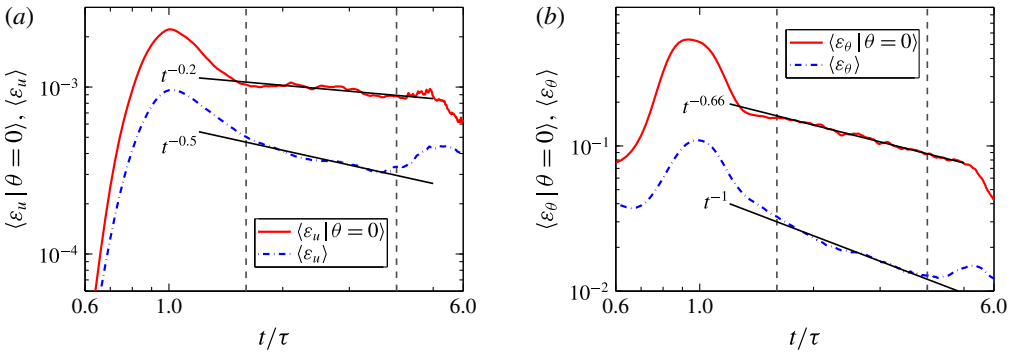

FIGURE 8. (*a*) Temporal evolution of the mean kinetic energy dissipation rate $\langle\varepsilon_u\rangle$ and its conditional value $\langle\varepsilon_u \,|\, \theta = 0\rangle$ calculated at the interfaces. The two vertical dashed lines mark the self-similarity turbulent range $1.6 \lesssim t/\tau \lesssim 4$ and the solid straight lines are the temporal scalings $t^{-0.2}$ and $t^{-0.5}$ for reference. (*b*) Temporal evolution of the mean thermal dissipation rate $\langle\varepsilon_\theta\rangle$ and its conditional value $\langle\varepsilon_\theta \,|\, \theta = 0\rangle$ calculated at the interfaces. The solid straight lines are the temporal scalings $t^{-0.66}$ and t^{-1} for reference.

enstrophy fluxes, and thus correspond to the strong correlations among the three fluxes. Based on this, the linelike structures may be used as a new indication of the time evolution of the mixing in RT turbulence.

As a preliminary try, we consider here the time behaviours of $\langle\varepsilon_u(\boldsymbol{x}, t) \,|\, \theta = 0\rangle$ and $\langle\varepsilon_\theta(\boldsymbol{x}, t) \,|\, \theta = 0\rangle$, the conditional average of the kinetic energy and thermal dissipation rates at the interfaces (i.e. the contour of $\theta = 0$), where

$$\varepsilon_u(\boldsymbol{x}, t) \equiv \nu[\partial u_j(\boldsymbol{x}, t)/\partial x_i]^2 \tag{3.6}$$

is the kinetic energy dissipation rate. Figures 8(*a*,*b*) show, respectively, the temporal evolution of $\langle\varepsilon_u \,|\, \theta = 0\rangle$ and $\langle\varepsilon_\theta \,|\, \theta = 0\rangle$. In the figures, we also plot the mean kinetic energy and thermal dissipation rates, $\langle\varepsilon_u\rangle$ and $\langle\varepsilon_\theta\rangle$, for comparison. As expected, one sees that both $\langle\varepsilon_u \,|\, \theta = 0\rangle$ and $\langle\varepsilon_\theta \,|\, \theta = 0\rangle$ are much larger than $\langle\varepsilon_u\rangle$ and $\langle\varepsilon_\theta\rangle$, respectively, indicating intense velocity and temperature gradients at the interfaces. In

the BO59 framework, Chertkov (2003) predicted $\langle \varepsilon_u \rangle \sim t^{-0.5}$ and $\langle \varepsilon_\theta \rangle \sim t^{-1}$. It is seen that in the self-similarity turbulent regime, as indicated by the two vertical dashed lines in figure 8, both $\langle \varepsilon_u \rangle$ and $\langle \varepsilon_\theta \rangle$ follow the theoretical predications well; this is also consistent with our previous results (Zhou 2013). On the other hand, $\langle \varepsilon_u \,|\, \theta = 0 \rangle$ and $\langle \varepsilon_\theta \,|\, \theta = 0 \rangle$ obtained at the interfaces both exhibit a less steep temporal scaling. The best fits to the data in the self-similarity range yield $\langle \varepsilon_u \,|\, \theta = 0 \rangle \sim t^{-0.2}$ and $\langle \varepsilon_\theta \,|\, \theta = 0 \rangle \sim t^{-0.66}$. As $\langle \varepsilon_u \,|\, \theta = 0 \rangle$ and $\langle \varepsilon_\theta \,|\, \theta = 0 \rangle$ are obtained from the most intense dissipation events, these new scaling laws may be attributed to the intermittent effects, as identified and discussed previously by Celani *et al.* (2006), Biferale *et al.* (2010), and Zhou (2013).

4. Conclusion

To conclude, we have analysed the energy and enstrophy transfer in 2D RT turbulence, by means of direct numerical simulations. Using FST, the fluxes of kinetic energy, thermal energy, and enstrophy across any given filter scale r are determined. With this information and the results obtained in previous works (Celani *et al.* 2006; Biferale *et al.* 2010; Boffetta *et al.* 2012; Zhou 2013), the cascade picture, in an averaged sense, of 2D RT turbulence can now be sketched as follows: on one hand, buoyancy forces provide kinetic energy on scale r, and then the kinetic energy is driven by an inverse cascade (figure 4*a* and Boffetta *et al.* 2012), due to the merging and grouping of buoyant structures. On the other hand, the temperature/density fluctuations follow a forward cascade from large to small scales (figure 5*a*). In the so-called inertial range, the above cascade processes are governed by two balances: one is the kinetic balance that the transport rate of the kinetic energy equals the buoyancy term (Zhou 2013), and the other is the scalar balance that the transfer rate of the temperature/density variance is scale-independent and is equal to its dissipation rate (inset of figure 5*a*). With these two balances, the BO59 scaling (1.1*a*,*b*) is yielded.

The statistical properties of the instantaneous local fluxes are also studied. It is found that locally there are regions of both inverse and direct cascades for all the three fluxes with asymmetric distributions. The fluctuations of $\Pi^{(r)}$, $N^{(r)}$ and $Z^{(r)}$ are more asymmetrically distributed at small scales than those at large scales. The analysis of the cross-correlation coefficients among the three local fluxes reveals that at small scales there is a strong correlation or anticorrelation between any two fluxes and the strength of this correlation or anticorrelation becomes weaker with increasing filter scale. These small-scale features are attributed to the mixing and dissipation near the interfaces between hot and cold plumes.

Acknowledgements

We thank N. T. Ouellette for helpful comments and discussions. This work was supported by Natural Science Foundation of China under grant nos. 11222222, 11572185 (Q.Z.), 11202122 (Y.-X.H.), 11272196 (Z.-M.L.) and 11332006 (Y.-L.L.), Innovation Program of Shanghai Municipal Education Commission under grant no. 13YZ008, Shanghai Shuguang Project under grant no. 13SG40, and Program for New Century Excellent Talents in University under grant no. NCET-13. Q.Z. wishes to acknowledge support given to him from the organization department of the CPC Central Committee through National Program for Support of Top-notch Young Professionals.

REFERENCES

ABARZHI, S. I. 2010*a* On fundamentals of Rayleigh–Taylor turbulent mixing. *Europhys. Lett.* **91**, 35001.

ABARZHI, S. I. 2010*b* Review of theoretical modelling approaches of Rayleigh–Taylor instabilities and turbulent mixing. *Phil. Trans. R. Soc. Lond.* A **368**, 1809–1828.

BIFERALE, L., MANTOVANI, F., SBRAGAGLIA, M., SCAGLIARINI, A., TOSCHI, F. & TRIPICCIONE, R. 2010 High resolution numerical study of Rayleigh–Taylor turbulence using a thermal lattice Boltzmann scheme. *Phys. Fluids* **22**, 115112.

BOFFETTA, G. 2007 Energy and enstrophy fluxes in the double cascade of two-dimensional turbulence. *J. Fluid Mech.* **589**, 253–260.

BOFFETTA, G. & ECKE, R. E. 2012 Two-dimensional turbulence. *Annu. Rev. Fluid Mech.* **44**, 427–451.

BOFFETTA, G., DE LILLO, F., MAZZINO, A. & MUSACCHIO, S. 2012 Bolgiano scale in confined Rayleigh–Taylor turbulence. *J. Fluid Mech.* **690**, 426–440.

BOFFETTA, G., MAZZINO, A., MUSACCHIO, S. & VOZELLA, L. 2009 Kolmogorov scaling and intermittency in Rayleigh–Taylor turbulence. *Phys. Rev.* E **79**, 065301(R).

BOFFETTA, G., MAZZINO, A., MUSACCHIO, S. & VOZELLA, L. 2010 Statistics of mixing in three-dimensional Rayleigh–Taylor turbulence at low Atwood number and Prandtl number one. *Phys. Fluids* **22**, 035109.

BOFFETTA, G. & MUSACCHIO, S. 2010 Evidence for the double cascade scenario in two-dimensional turbulence. *Phys. Rev.* E **82**, 016307.

BORUE, V. & ORSZAG, S. A. 1998 Local energy flux and subgrid-scale statistics in three-dimensional turbulence. *J. Fluid Mech.* **366**, 1–31.

CABOT, W. H. & COOK, A. W. 2006 Reynolds number effects on Rayleigh–Taylor instability with possible implications for type Ia supernovae. *Nat. Phys.* **2**, 562–568.

CELANI, A., MAZZINO, A. & VOZELLA, L. 2006 Rayleigh–Taylor turbulence in two dimensions. *Phys. Rev. Lett.* **96**, 134504.

CHEN, S.-Y., ECKE, R. E., EYINK, G. L., RIVERA, M., WAN, M.-P. & XIAO, Z.-L. 2006 Physical mechanism of the two-dimensional inverse energy cascade. *Phys. Rev. Lett.* **96**, 084502.

CHEN, S.-Y., ECKE, R. E., EYINK, G. L., WANG, X. & XIAO, Z.-L. 2003 Physical mechanism of the two-dimensional enstrophy cascade. *Phys. Rev. Lett.* **91**, 214501.

CHERTKOV, M. 2003 Phenomenology of Rayleigh–Taylor turbulence. *Phys. Rev. Lett.* **91**, 115001.

CHUNG, D. & PULLIN, D. I. 2010 Direct numerical simulation and large-eddy simulation of stationary buoyancy-driven turbulence. *J. Fluid Mech.* **643**, 279–308.

CLERCX, H. J. H. & VAN HEIJST, G. J. F. 2009 Two-dimensional Navier–Stokes turbulence in bounded domains. *Appl. Mech. Rev.* **62**, 020802.

DALZIEL, S. B., LINDEN, P. F. & YOUNGS, D. L. 1999 Self-similarity and internal structure of turbulence induced by Rayleigh–Taylor instability. *J. Fluid Mech.* **399**, 1–48.

DIMONTE, G., YOUNGS, D. L., DIMITS, A., WEBER, S., MARINAK, M., WUNSCH, S., GARASI, C., ROBINSON, A., ANDREWS, M. J., RAMAPRABHU, P. *et al.* 2004 A comparative study of the turbulent Rayleigh–Taylor instability using high-resolution three-dimensional numerical simulations: The Alpha-Group collaboration. *Phys. Fluids* **16**, 1668–1693.

EYINK, G. L. 1995 Local energy flux and the refined similarity hypothesis. *J. Stat. Phys.* **78**, 335–351.

GERMANO, M. 1992 Turbulence: the filtering approach. *J. Fluid Mech.* **238**, 325–336.

HUANG, Y.-X. & ZHOU, Q. 2013 Counter-gradient heat transport in two-dimensional turbulent Rayleigh–Bénard convection. *J. Fluid Mech.* **737**, R3.

ISOBE, H., MIYAGOSHI, T., SHIBATA, K. & YOKOYAMA, T. 2005 Filamentary structure on the Sun from the magnetic Rayleigh–Taylor instability. *Nature* **434**, 478–481.

KELLEY, D. H. & OUELLETTE, N. T. 2011 Spatiotemporal persistence of spectral fluxes in two-dimensional weak turbulence. *Phys. Fluids* **23**, 115101.

LIAO, Y. & OUELLETTE, N. T. 2013 Spatial structure of spectral transport in two-dimensional flow. *J. Fluid Mech.* **725**, 281–2988.

LIAO, Y. & OUELLETTE, N. T. 2014 Geometry of scale-to-scale energy and enstrophy transport in two-dimensional flow. *Phys. Fluids* **26**, 045103.

LIU, J.-G., WANG, C. & JOHNSTON, H. 2003 A fourth order scheme for incompressible Boussinesq equations. *J. Sci. Comput.* **18**, 253–285.

LIU, S., MENEVEAU, C. & KATZ, J. 1994 On the properties of similarity subgrid-scale models as deduced from measurements in a turbulent jet. *J. Fluid Mech.* **275**, 83–119.

LOHSE, D. & XIA, K.-Q. 2010 Small-scale properties of turbulent Rayleigh–Bénard convection. *Annu. Rev. Fluid Mech.* **42**, 335–364.

MATSUMOTO, T. 2009 Anomalous scaling of three-dimensional Rayleigh–Taylor turbulence. *Phys. Rev.* E **79**, 055301(R).

NI, R., VOTH, G. A. & OUELLETTE, N. T. 2014 Extracting turbulent spectral transfer from under-resolved velocity fields. *Phys. Fluids* **26**, 105107.

QIU, X., LIU, Y.-L. & ZHOU, Q. 2014 Local dissipation scales in two-dimensional Rayleigh–Taylor turbulence. *Phys. Rev.* E **90**, 043012.

RIVERA, M. K., DANIEL, W. B., CHEN, S. Y. & ECKE, R. E. 2003 Energy and enstrophy transfer in decaying two-dimensional turbulence. *Phys. Rev. Lett.* **90**, 104502.

SOULARD, O. 2012 Implications of the Monin–Yaglom relation for Rayleigh–Taylor turbulence. *Phys. Rev. Lett.* **109**, 254501.

SOULARD, O. & GRIFFOND, J. 2012 Inertial-range anisotropy in Rayleigh–Taylor turbulence. *Phys. Fluids* **24**, 025101.

TALEYARKHAN, R. P., WEST, C. D., CHO, J. S. JR, LAHEY, R. T., NIGMATULIN, R. I. & BLOCK, R. C. 2002 Evidence for nuclear emissions during acoustic cavitation. *Science* **295**, 1868–1873.

VLADIMIROVA, N. & CHERTKOV, M. 2009 Self-similarity and universality in Rayleigh–Taylor, Boussinesq turbulence. *Phys. Fluids* **21**, 015102.

WAN, M.-P., XIAO, Z.-L., MENEVEAU, C., EYINK, G. L. & CHEN, S.-Y. 2010 Dissipation-energy flux correlations as evidence for the Lagrangian energy cascade in turbulence. *Phys. Fluids* **22**, 061702.

WEINAN, E. & LIU, J.-G. 1996 Vorticity boundary condition and related issues for finite difference schemes. *J. Comput. Phys.* **124**, 368–382.

WILSON, P. N. & ANDREWS, M. J. 2002 Spectral measurements of Rayleigh–Taylor mixing at small Atwood number. *Phys. Fluids* **14**, 938–945.

XIAO, Z., WAN, M., CHEN, S. & EYINK, G. L. 2009 Physical mechanism of the inverse energy cascade of two-dimensional turbulence: a numerical investigation. *J. Fluid Mech.* **619**, 1–44.

ZHOU, Q. 2013 Temporal evolution and scaling of mixing in two-dimensional Rayleigh–Taylor turbulence. *Phys. Fluids* **25**, 085107.

ZHOU, Y. 2001 A scaling analysis of turbulent flows driven by Rayleigh–Taylor and Richtmyer–Meshkov instabilities. *Phys. Fluids* **13**, 538–543.

ZINGALE, M., WOOSLEY, S. E., RENDLEMAN, C. A., DAY, M. S. & BELL, J. B. 2005 Three-dimensional numerical simulations of Rayleigh–Taylor unstable flames in type Ia supernovae. *Astrophys. J.* **632**, 1021–1034.